frontiers in Microbiology

ORIGINAL RESEARCH
published: 22 June 2016
doi: 10.3389/fmicb.2016.00918

Transhydrogenase and Growth Substrate Influence Lipid Hydrogen Isotope Ratios in *Desulfovibrio alaskensis* G20

William D. Leavitt[1], Theodore M. Flynn[2], Melanie K. Suess[1] and Alexander S. Bradley[1,3]**

[1] Department of Earth and Planetary Sciences, Washington University in St. Louis, Saint Louis, MO, USA, [2] Biosciences Division, Argonne National Laboratory, Argonne, IL, USA, [3] Division of Biology and Biomedical Sciences, Washington University in St. Louis, Saint Louis, MO, USA

OPEN ACCESS

Edited by:
Shuhei Ono, Massachusetts Institute of Technology, USA

Reviewed by:
John Senko, The University of Akron, USA
Alex Sessions, California Institute of Technology, USA

***Correspondence:**
William D. Leavitt
wleavitt@eps.wustl.edu;
Alexander S. Bradley
abradley@eps.wustl.edu

Specialty section:
This article was submitted to Microbiological Chemistry and Geomicrobiology, a section of the journal Frontiers in Microbiology

Received: *14 February 2016*
Accepted: *27 May 2016*
Published: *22 June 2016*

Citation:
Leavitt WD, Flynn TM, Suess MK and Bradley AS (2016) Transhydrogenase and Growth Substrate Influence Lipid Hydrogen Isotope Ratios in Desulfovibrio alaskensis G20. Front. Microbiol. 7:918. doi: 10.3389/fmicb.2016.00918

Microbial fatty acids preserve metabolic and environmental information in their hydrogen isotope ratios ($^2H/^1H$). This ratio is influenced by parameters that include the $^2H/^1H$ of water in the microbial growth environment, and biosynthetic fractionations between water and lipid. In some microbes, this biosynthetic fractionation has been shown to vary systematically with central energy metabolism, and controls on fatty acid $^2H/^1H$ may be linked to the intracellular production of NADPH. We examined the apparent fractionation between media water and the fatty acids produced by *Desulfovibrio alaskensis* G20. Growth was in batch culture with malate as an electron donor for sulfate respiration, and with pyruvate and fumarate as substrates for fermentation and for sulfate respiration. A larger fractionation was observed as a consequence of respiratory or fermentative growth on pyruvate than growth on fumarate or malate. This difference correlates with opposite apparent flows of electrons through the electron bifurcating/confurcating transhydrogenase NfnAB. When grown on malate or fumarate, mutant strains of *D. alaskensis* G20 containing transposon disruptions in a copy of *nfnAB* show different fractionations than the wild type strain. This phenotype is muted during fermentative growth on pyruvate, and it is absent when pyruvate is a substrate for sulfate reduction. All strains and conditions produced similar fatty acid profiles, and the $^2H/^1H$ of individual lipids changed in concert with the mass-weighted average. Unsaturated fatty acids were generally depleted in ^2H relative to their saturated homologs, and anteiso-branched fatty acids were generally depleted in ^2H relative to straight-chain fatty acids. Fractionation correlated with growth rate, a pattern that has also been observed in the fractionation of sulfur isotopes during dissimilatory sulfate reduction by sulfate-reducing bacteria.

Keywords: compound specific hydrogen isotopes, transhydrogenase, lipid biomarkers, dissimilatory sulfate reduction

Abbreviations: BLAST, basic local alignment tool search; BLASTP, basic local alignment tool search protein; EDTA, ethylenediaminetetraacetic acid; NAD(H), nicotinamide adenine dinucleotide; NADP(H), nicotinamide adenine dinucleotide phosphate; RMS, root mean square; V-SMOW, Vienna standard mean ocean water.

INTRODUCTION

The structures and isotopic compositions of lipids preserve information about organisms that can be archived in sediments and rocks over geological time scales. Understanding how to interpret this information is a central task of organic geochemistry. Lipid structures can be affiliated to particular groups of organisms (Pearson, 2014), and ratios of carbon isotopes in lipids record information about carbon sources and assimilation pathways (Smith and Epstein, 1970; Hayes, 2001). The ratio of hydrogen isotopes (deuterium/protium = $^2H/^1H$) in lipids derived from environmental samples has been observed to relate to the $^2H/^1H$ of environmental water (Hayes, 2001; Sauer et al., 2001). More recently, it was shown in a range of aerobic microorganisms that the fractionation of hydrogen isotopes between media water and lipids varied with changes in growth substrate (Zhang et al., 2009). Experiments with anaerobes have shown less systematic changes in lipid $^2H/^1H$ as a function of energy metabolism, although strong differences have been observed in lipid $^2H/^1H$ of organisms in pure culture versus co-cultures with another organism (Dawson et al., 2015; Osburn et al., in review).

Observations that lipid $^2H/^1H$ varies as a function of growth substrate in many microorganisms raises the question of what specific metabolic mechanisms are responsible. Zhang et al. (2009) considered several explanations, and through a process of elimination, deduced that observed differences in lipid $^2H/^1H$ must be a consequence of differences in the NAD(P)H that serves as a hydride donor during lipid biosynthesis. These authors pointed out that cells have multiple pathways for producing NAD(P)H, and that the relative importance of each of these mechanisms varies with differences in growth conditions. One mechanism considered was alteration of the $^2H/^1H$ ratio of the transferable hydride in NAD(P)H by transhydrogenase enzymes. This suggestion stems from two key observations. First, up to half of the hydrogen atoms in microbial lipids are derived directly from NADPH during biosynthesis (Saito et al., 1980; Jackson, 2003). Second, *in vitro* observations of the hydrogen isotope fractionation imparted by transhydrogenase suggest that it is very large (>800‰; Bizouarn et al., 1995; Venning et al., 1998; Jackson et al., 1999).

In this study, we vary substrates and use mutant strains to investigate the importance of a transhydrogenase (NADH-dependent reduced ferredoxin:NADP oxidoreductase; NfnAB) on the lipid $^2H/^1H$ ratios in an anaerobic microorganism, *Desulfovibrio alaskensis* G20. Recent work has suggested that NfnAB plays an important role in energy conservation in this microbe (Price et al., 2014). The role of NfnAB varies as a function of the growth substrate. During growth on malate, for example, NfnAB is predicted to catalyze an electron bifurcation reaction (Buckel and Thauer, 2013) in which NADPH reduces ferredoxin and NAD^+ to produce NADH (**Figure 1**). Conversely, during growth on pyruvate, NfnAB is predicted to catalyze electron confurcation and the production of NADPH from NADH, $NADP^+$, and reduced ferredoxin. The importance of this transhydrogenase to anaerobic energy metabolism may be critical to understanding lipid H-isotope signatures. Since the transhydrogenase reaction catalyzed by NfnAB is predicted to occur in opposite directions during growth on pyruvate versus that on malate, the lipids produced under each condition should have different $^2H/^1H$ ratios if NfnAB is indeed a significant source of isotope fractionation for intracellular hydrogen. Furthermore, the role of NfnAB in hydrogen isotope fractionation can be further explored using mutant strains of *D. alaskensis* G20 in which the NfnAB-2 loci have been disrupted.

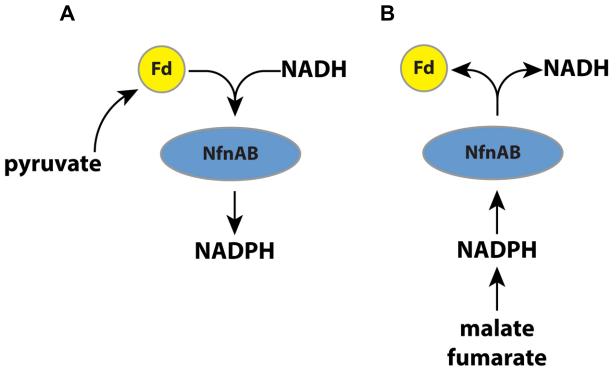

FIGURE 1 | (A) A schematic pathway of electron flow during pyruvate respiration or fermentation in wild type *D. alaskensis* G20. Electrons are transferred from pyruvate through ferredoxin and NADPH, and NfnAB catalyzes electron confurcation, producing NADPH. Mutation of NfnAB inhibits this reaction and may result in a relative NADPH deficiency. **(B)** A schematic of electron flow during fumarate respiration, malate respiration, or fumarate fermentation. Mutation of NfnAB inhibits this reaction and may result in a relative NADPH surplus.

MATERIALS AND METHODS

Strains, Growth Media, Culture Conditions, and Biomass Sampling

Wild type *D. alaskensis* G20 was obtained along with two mutant strains from the library collection at Lawrence Berkeley National Laboratory. Each mutant contains a Tn5 transposon insertion into a gene of interest. These insertions (Kuehl et al., 2014) were into the genes *nfnA*-2 at locus Dde_1250 (strain JK00256) and *nfn*B-2 at locus Dde_1251 (JK01775). Hereafter, these strains are referred to as the *nfnA*-2 and *nfnB*-2 mutants. These loci encode the subunits for one of two paralogs of NfnAB in *D. alaskensis* G20.

All strains were resuscitated from 10% glycerol freezer stocks stored at −80°C. Resuscitated strains were inoculated into serum bottles containing approximately 50 ml of a rich lactate/sulfate medium containing yeast extract (MOY_LS) and incubated at 30°C. After reaching stationary phase, strains were then serially transferred three times in a defined lactate/sulfate (80 mM/40 mM) medium (MO_LS). Late-log phase cultures of the third transfer were diluted 1−100 into duplicate bottles for each isotope fractionation experiment. There were five experimental growth conditions, which combined an electron donor and 40 mM sulfate (for sulfate respiration),

or an electron donor alone for fermentation. The five conditions were pyruvate/sulfate respiration, malate/sulfate respiration, fumarate/sulfate respiration, pyruvate fermentation, and fumarate fermentation.

The basal growth medium recipe (MO) was as follows: 8 mM magnesium chloride, 20 mM ammonium chloride, 0.6 mM calcium chloride, 6 mL/L trace elements solution (see below), 0.12 mM of $FeCl_2$ (125 mM) + EDTA (250 mM) stock solution, 30 mM Tris–HCl (2 M, pH 7.4 stock). Sodium thioglycolate (0.12 g/L) was added as a reductant following initial degassing. For initial cultures revived from freezer stocks, the MO medium was supplemented with yeast extract (0.1% w/v) from an anoxic sterile stock, thereby designated MOY medium. Media were made anaerobic by degassing with O_2-free N_2 that had been filtered through sterile 0.22 μm syringe filters. Solutions were degassed for 2 h/L. The pH of the final medium was adjusted to 7.2 using sterile and anoxic HCl or NaOH, autoclave-sterilized, and then cooled under sterile O_2-free N_2. After cooling, phosphate solution was added to a final concentration of 2 mM from a sterile, anoxic stock solution of K_2HPO_4 + NaH_2PO_4. Thauer's vitamins were added from a 1000× stock (Rabus et al., 2015). The initial concentration of sulfate was always 40 mM (except in fermentation experiments) and was added directly to the medium from a sterile and anoxic stock solution of Na_2SO_4 solution. Electron donors (sodium lactate, sodium pyruvate, malic acid, or sodium fumarate) were prepared separately as 1 M stocks in MilliQ water, adjusted to a pH of 7.2, and degassed in a manner similar to the basal media. These anoxic stocks were then added to the basal media using aseptic technique.

Growth rate was determined by monitoring changes in optical density (OD_{600}) over time for each experiment. Replicate cultures were tracked through log-phase and into early stationary phase, at which point they were harvested for biomass. Growth rates were calculated using a modified logistic equation (Rabus et al., 2006) and averaged across the apparent log-phase of growth. In experiments showing diauxic growth, we calculated a weighted average growth rate, where weighting accounts for the amount of biomass produced during each growth interval.

Duplicate 50 mL cultures were harvested at the onset of early stationary phase by opening the serum bottles, decanting the remainder of each serum bottle (>40 mL) into sterile 50 mL conical tubes, and centrifuging at 5000 rpm at 5°C for 30 min. Spent medium was decanted into a fresh 50 mL tube and frozen at −80°C for later analysis of the isotopic composition of water therein. The biomass pellet was frozen at −80°C, transferred to a pre-baked and weighed 4 mL borosilicate glass vial, lyophilized, and weighed.

Fatty Acid Extraction, Identification, and Quantitation

Samples were simultaneously extracted and derivatized to fatty acid methyl ethers (FAMEs) by adding a mixture of hexane, methanol, and acetyl chloride to the lyophilized cell pellet, followed by heating at 100°C for 10 min, and extraction with hexane (Rodriguez-Ruiz et al., 1998; Zhang et al., 2009). This procedure was also concurrently performed on two isotope standards, myristic acid and phthalic acid, for which the δ^2H of non-exchangeable hydrogen has been determined (Qi and Coplen, 2011). Each sample was reacted with acid-activated copper shot to remove elemental sulfur, and then concentrated under a stream of dry hydrocarbon-free nitrogen.

Individual FAMEs were analyzed using a HP 7890 gas chromatograph fitted with a split/splitless injector operated in splitless mode, equipped with a J&W DB-5 fused silica capillary column (30 m length, 0.25-mm inner diameter, and 0.25-μm film thickness) and coupled to an Agilent 6973 mass selective detector. FAME identifications were based on mass spectra and retention times and are reported in Supplementary Table S1. Retention times were converted to Kovats retention indices by comparison to a mix of *n*-alkanes, and compared to the retention indices of published fatty acids (Taylor and Parkes, 1983; Dickschat et al., 2011). Double bond locations were identified by converting unsaturated fatty acids to their dimethyl disulfide adducts (Nichols et al., 1986). Abundances were determined by peak area as calculated in Chemstation (Agilent Technologies, Santa Clara, CA, USA) relative to a known amount of co-injected methyl tetracosanoate (C24:0).

Isotopic Measurements and Data Handling

Hydrogen-isotopic compositions of individual FAMEs were determined using a TraceGC gas chromatograph fitted with a column identical to that on the Agilent GC, and coupled to a Thermo Scientific Delta V Plus isotope-ratio-monitoring mass spectrometer via a Thermo GC-Isolink pyrolysis interface at 1400°C. Column temperature was initially 60°C and was increased at a rate of 6°C min^{-1} until reaching a final temperature of 320°C. Hydrogen isotope ratios of individual lipids were determined relative to coinjected methyl tetracosanoate (C24:0) of known isotopic composition, provided by Dr. A. Schimmelmann (Indiana University). Instrumental precision was regularly monitored by analyzing the δ^2H on external standard mixtures of FAMEs and of *n*-alkanes with previously determined isotopic composition (V-SMOW), also purchased from Dr. Schimmelmann (Indiana University). Over the measurement period the mean RMS error on a mixture of eight FAMEs was 5.5‰ (n = 286). Samples were discarded if they were not bracketed by injections of FAMEs mixture with an RMS better than 7‰. H_3 factors were determined daily and had a mean value of 2.98 ± 0.3 ppm/nA. All FAME isotopic compositions were corrected by mass balance for the hydrogen present in the methyl group, calculated from the myristic acid and phthalic acid isotopic standards. Samples were re-injected (pseudoreplicates) three to six times, and errors were propagated following established methods (Polissar and D'Andrea, 2014). Statistical analyses were performed in either Prism (GraphPad Software, Inc., La Jolla, CA, USA) or R (R Core Team, 2015).

All $^2H/^1H$ ratios are reported as δ^2H values relative to V-SMOW, and fractionations are reported as apparent fractionations between media water and lipid by the equation: $^2\varepsilon_{lipid-water} = (\alpha_{lipid-water} - 1)$, where $\alpha = [(\delta^2H_{lipid} + 1)/(\delta^2H_{water} + 1)]$ and are reported in ‰ (Coplen et al., 2002). The δ^2H_{water} of growth media water was measured using a Picarro L2130-*i* cavity ring-down spectrometer at Northwestern University.

Comparative Analysis of *nfnAB* Sequences

We constructed a gene tree of *nfnAB* sequences by retrieving data from two public repositories of annotated genomes: the SEED (Overbeek et al., 2014) and IMG (Markowitz et al., 2012). For this study, we restricted sequences to those also found in the subsystem "NADH-dependent reduced ferredoxin:$NADP^+$ oxidoreductase" in the SEED (197 total sequences) and manually refined the list to sequences from known sulfate reducers, methanogens, and other anaerobes. Sequences from organisms known to contain *nfnAB* but not present in the SEED were added manually using a targeted amino acid BLAST search of that organism's genome in the IMG database. This resulted in a total of 105 *nfnAB* sequences closely related to that of *D. alaskensis* G20 using established criteria (Rost, 1999; Marti-Renom et al., 2000), with >40% amino acid identity and BLASTP percent identities ranging from 45 to 77%. *D. alaskensis* G20 itself has two copies of *nfnAB* that share 85% amino acid identity. A multiple sequence alignment of the 105 putative *nfnAB* sequences was created using MUSCLE (Edgar, 2004) and checked manually using AliView (Larsson, 2014). Alignments in FASTA format are available to download in the Supplementary Materials. Pairwise distances for construction of a phylogenetic tree were calculated using the RAxML maximum likelihood algorithm (Stamatakis, 2006) with the program raxmlGUI (Silvestro and Michalak, 2012). The tree itself was generated using the Interactive Tree of Life software (Letunic and Bork, 2011).

RESULTS

Growth Rates

Growth experiments revealed distinct physiological and isotopic phenotypes among the wild type and mutant strains of *D. alaskensis* G20. Growth rates are reported in **Table 1** and growth curves are plotted in **Figure 2**.

Some growth conditions showed clear phenotypic differences between the *D. alaskensis* G20 wild type and the two *nfnAB-2* mutants. Each strain was able to grow as a sulfate reducer using malate as an electron donor, but the growth rate of the mutants was only 22% that of the wild type. Similarly, with fumarate as an electron donor coupled to sulfate reduction, mutant growth rate was roughly 10% that of the wild type. A repression in growth rate (22% of wild type) was also apparent when the strains were grown as fumarate fermenters, in the absence of sulfate. Under all of these conditions, the final optical density of the mutant cultures was less than that of the wild type (**Figure 2**). The mutant strains exhibited diauxic growth under each of these growth conditions whereas the wild type did not (**Figure 2**).

Lipid Profiles

We quantified the abundance of fatty acid structures in each of the three strains under all five experimental conditions (pyruvate/sulfate, malate/sulfate, fumarate/sulfate, fumarate fermentation, or pyruvate fermentation). Fatty acids ranged in carbon number from 14 to 18, and both saturated and monounsaturated fatty acids were present. Branched-chain fatty acids of the iso- and anteiso-series are present in all three strains under all five experimental conditions. Branched fatty acids contained a total of 15–18 carbons, and in some cases contained a double bound.

Differences in the lipid profiles of the mutant relative to the wild type were apparent only under the three conditions in which the mutant showed a growth defect: malate/sulfate, fumarate/sulfate, and fumarate fermentation (**Figures 3B–D**). During growth on malate/sulfate, the *nfn*AB-2 mutant strains contain a higher proportion of anteiso-C17:0, and a lower proportion of C16:0, C18:0, and iso-C15:0 fatty acids. A similar pattern is seen in the mutants during growth on fumarate/sulfate and during fumarate fermentation, although the C18 patterns are slightly different. Differences in the abundance of anteiso-C17:0 fatty acid is most pronounced in these three growth conditions. In contrast, during both respiratory and fermentative growth on pyruvate, the fatty acid profile of the wild type and mutants were nearly identical (**Figures 3A,E**). Across all strains and conditions, there is a weak inverse correlation between the proportion of branched fatty acids

TABLE 1 | Interval-weighted growth rates of *D. alaskensis* G20 wild type and *nfnAB-2* transhydrogenase mutants on different substrates during sulfate respiration or substrate fermentation.

Weighted average growth rates		
Treatment	**Strain**	**μ_{avg} (per h)**
Pyruvate + sulfate	Wild type	0.154 ± 0.029
	nfnA-2	0.172 ± 0.029
	nfnB-2	0.168 ± 0.035
Malate + sulfate	Wild type	0.067 ± 0.007
	nfnA-2	0.014 ± 0.006
	nfnB-2	0.015 ± 0.004
Fumarate + sulfate	Wild type	0.085 ± 0.012
	nfnA-2	0.011 ± 0.002
	nfnB-2	0.007 ± 0.006
Fumarate fermentation	Wild type	0.057 ± 0.007
	nfnA-2	0.010 ± 0.002
	nfnB-2	0.015 ± 0.004
Pyruvate fermentation	Wild type	0.131 ± 0.007
	nfnA-2	0.120 ± 0.001
	nfnB-2	0.149 ± 0.012

*The range in rate is larger for experiments that exhibited bi-phasic (diauxic) growth patterns (e.g., fumarate + sulfate), as is apparent from the growth curves (**Figure 2**).*

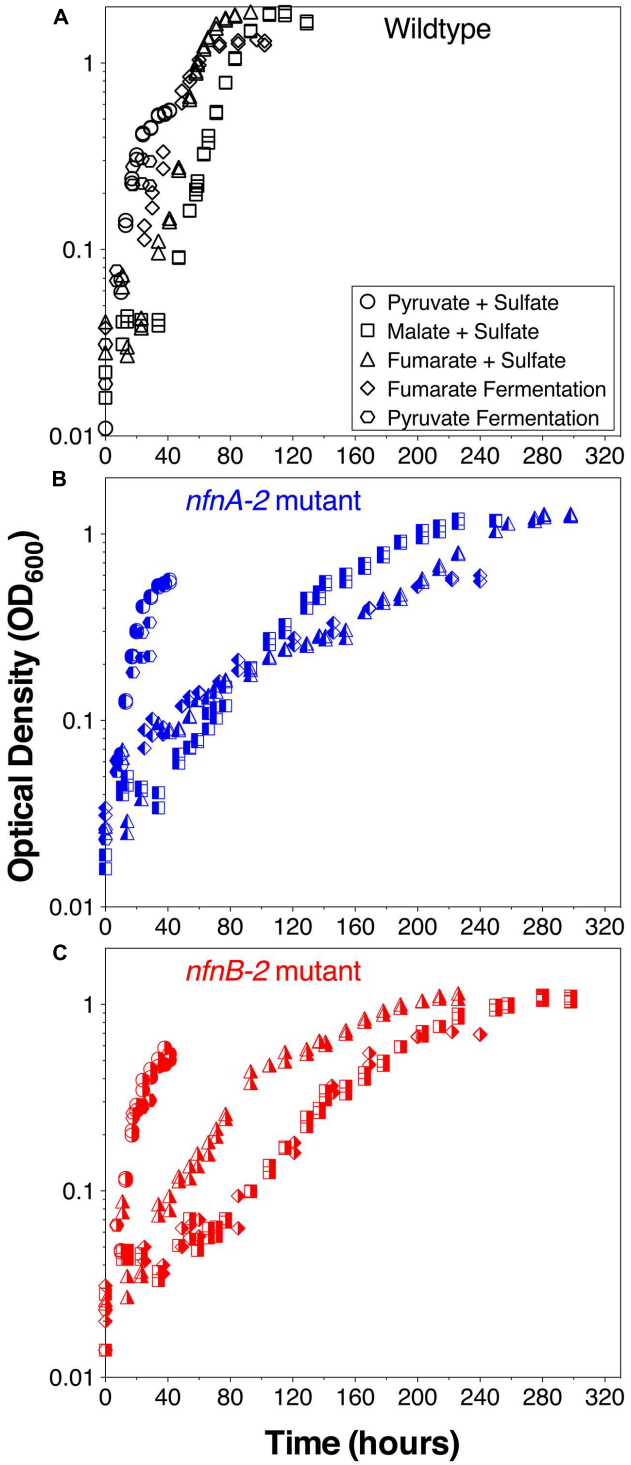

FIGURE 2 | Growth curves for *D. alaskensis* G20 wild type and transhydrogenase mutants. (A) Wild type, **(B)** *nfnA-2* transposon mutant, and **(C)** *nfnB-2* transposon mutant, each under all five-condition sets tested (denoted in the legends). Each symbol represents the average of biological duplicate 50 mL cultures. Error bars are smaller than the symbols in all cases. Samples for lipid and isotopic analysis were extracted after the final time-point indicated on this plot, all in early stationary phase.

(Supplementary Figure S1A) or the ratio of anteiso- to iso-branched compounds (Supplementary Figure S1B), in each case relative to the mass weighted fractionation. Data used to generate these plots are deposited in a permanent repository at http://dx.doi.org/10.6084/m9.figshare.2132731.

Lipid $^2H/^1H$ Fractionations

We calculated δ^2H_{total} as the weighted average of the δ^2H_{lipid} of each individual fatty acid pool produced in each strain. We then calculated a total apparent fractionation ($^2\varepsilon_{total}$) for the fatty acid pool (Sessions and Hayes, 2005). The results are shown in **Figure 4**. Apparent fractionations produced by the wild type strain were not discernable between pyruvate/sulfate respiration ($^2\varepsilon_{total} = -171‰$) and pyruvate fermentation ($^2\varepsilon_{total} = -168‰$). Similarly, both *nfn* mutants have $^2\varepsilon_{total} = -171‰$ when grown by pyruvate/sulfate respiration. However, *nfn* mutants that grew by fermenting pyruvate had $^2\varepsilon_{total} = -160‰$ for the *nfnA*-2 mutant and $^2\varepsilon_{total} = -162‰$ for the *nfnB*-2 mutant.

Differences in $^2\varepsilon_{total}$ were more pronounced in the other growth conditions. In comparison to growth on pyruvate, the wild type strain showed less negative $^2\varepsilon_{total}$ as a consequence of malate/sulfate growth ($^2\varepsilon_{total} = -143‰$), fumarate/sulfate growth ($^2\varepsilon_{total} = -135‰$), and fumarate fermentation ($^2\varepsilon_{total} = -142‰$). The *nfn* mutants showed even stronger isotopic phenotypes. The *nfnA*-2 mutant had less negative $^2\varepsilon_{total}$ than the wild type during growth on malate/sulfate ($^2\varepsilon_{total} = -82‰$), fumarate/sulfate ($^2\varepsilon_{total} = -103‰$), and fumarate ($^2\varepsilon_{total} = -108‰$). The magnitude of fractionation by the *nfnB*-2 mutant was consistently less than that of both the wild type and the *nfnA*-2 mutant on malate/sulfate ($^2\varepsilon_{total} = -59‰$), fumarate/sulfate ($^2\varepsilon_{total} = -72‰$), and fumarate ($^2\varepsilon_{total} = -72‰$).

The δ^2H_{lipid} of individual lipids can help explain some of these patterns. Most lipids from our cultures were depleted in deuterium by between −50‰ and −250‰ relative to the water in the growth medium. **Figure 5** summarizes the results from each strain. The various lipid structures produced by each strain had a wide range of $^2\varepsilon_{lipid}$, but isotopic ordering among lipids was remarkably consistent. **Figure 5** shows $^2\varepsilon_{lipid}$ values for the most abundant lipids in each combination of strain and culture conditions. For all three strains, across nearly every culture condition, the fatty acid with the largest $^2\varepsilon_{lipid}$ was C16:1. The exceptions to this were produced by the pyruvate fermentation experiments, in which the largest $^2\varepsilon_{lipid}$ observed was in anteiso-C17:1 in all three strains, and by fumarate fermentation by the mutants, where the C16:1 was in too low abundance for δ^2H measurements (**Figure 5**). Across all sulfate reduction experiments, fatty acids containing a double bond were nearly always depleted relative to their saturated homolog. This was true for both the straight chained and branched fatty acids. Differences in δ^2H were larger between C16 and C16:1 than between C18 and C18:1, driven by the particularly strong ^2H depletion in C16:1. This pattern was muted in the fermentation experiments. We also found that saturated anteiso- branched fatty acids produced during sulfate reduction were always depleted relative to straight-chain fatty acids. This pattern did not hold for unsaturated

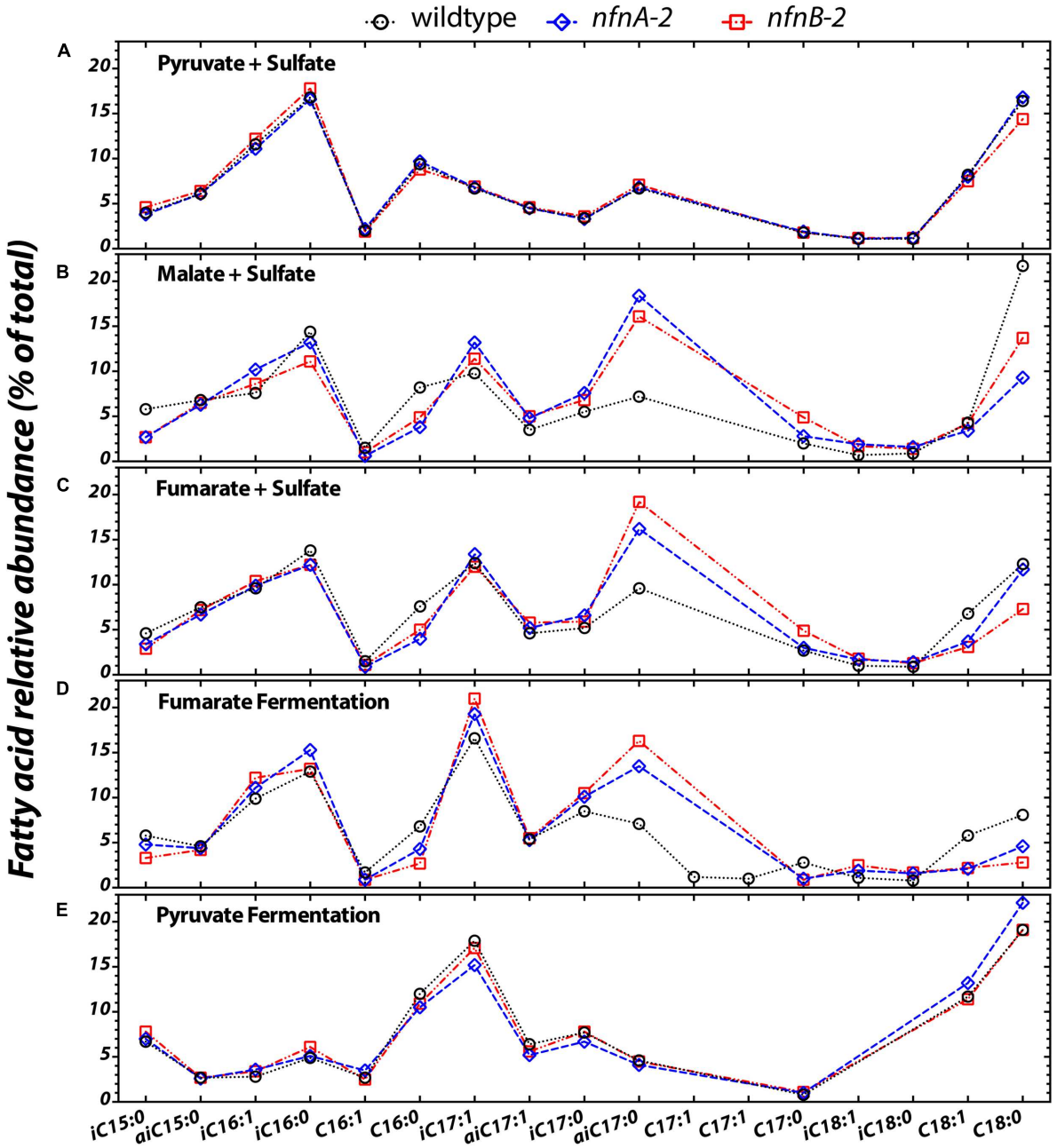

FIGURE 3 | The relative abundance of each fatty acid (% of total) from each strain under the five different growth conditions tested (A–E). Sample key: wild type (black circles, dotted lines) or *nfnAB-2* transhydrogenase insertion–deletion mutants, *nfnA-2* (blue diamonds, dashed lines) and *nfnB-2* (red squares, dash-dotted lines). The double bond in *n*-C16, *iso*-C16, *iso*-C17, *anteiso*-C17 is located at the Δ9 carbon, and on the *n*-C18 and *iso*-C18 at the Δ11 carbon. Double bond position in each of the two C17:1 peaks was not identified. Each symbol represents the average of biological replicates for each strain given that condition set, and the standard error of individual fatty acid quantifications is <0.5% between biological replicates (error bars are significantly smaller than the symbols).

anteiso-fatty acids or for lipids produced during fermentation. Saturated iso-branched fatty acids had similar δ^2H as saturated straight-chain fatty acids. The lipid with the least negative $^2\varepsilon_{lipid}$ was iso-C18:0 (**Figure 5**). When produced under certain sulfate reducing conditions, this lipid was enriched in ^2H relative to media water ($^2\varepsilon_{lipid} > 0‰$). Under fermentative conditions, this lipid was produced in insufficient abundance to measure δ^2H_{lipid}.

The regular ordering of lipid δ^2H values suggests that the variations in $^2\varepsilon_{total}$ were mainly a function of a systematic change in $^2\varepsilon$ from one condition to another rather than changes in the relative proportion of individual lipids that are particularly

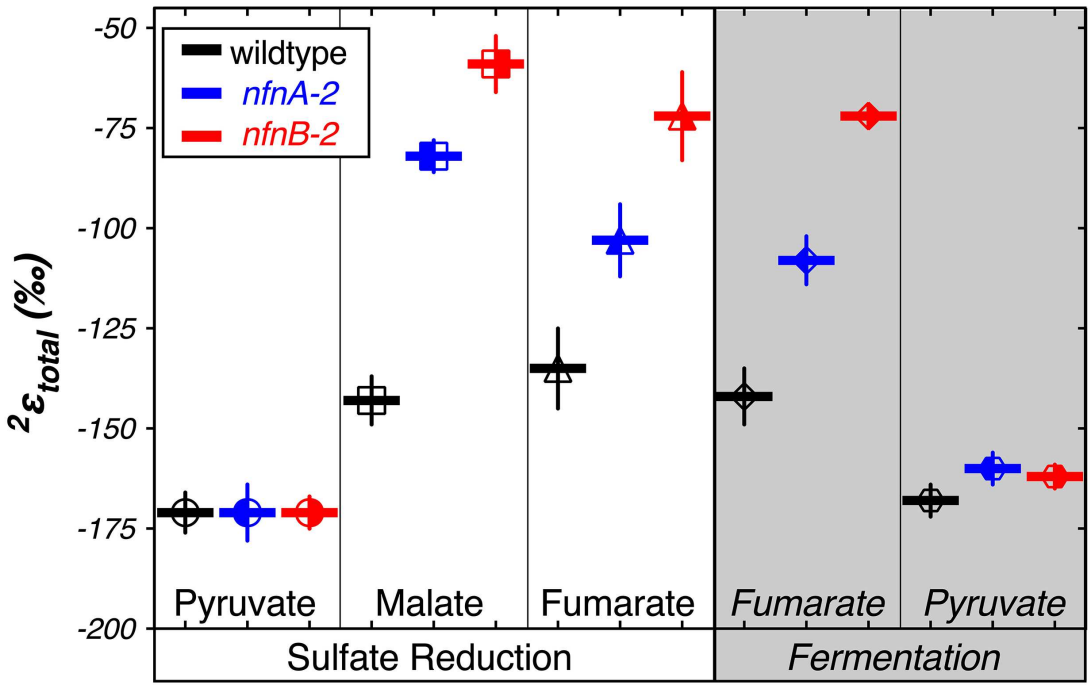

FIGURE 4 | Hydrogen isotope fractionation between media water and the mass-weighted lipid pool ($^2\varepsilon_{total}$) is plotted for each treat. Vertical bars are standard errors on the mean (SEM). Symbols and colors are consistent with **Figures 2** and **3**.

enriched or depleted. In **Figure 5**, the thick black line and circles show $^2\varepsilon_{total}$, highlighting the relationship between $^2\varepsilon_{lipid}$ and $^2\varepsilon_{total}$ for each strain and culture condition. With few exceptions, a consistent pattern emerged in the relative fractionation of each lipid relative to the weighted average. Together, **Figures 4** and **5** indicate the presence of significant differences between the wild type and mutants for growth on malate/sulfate, fumarate/sulfate, or fumarate fermentation, while little to no difference existed between strains grown on pyruvate/sulfate or pyruvate fermentation.

We examined whether changes in the abundance of particular lipids were correlated with each other, with growth rate, or with $^2\varepsilon_{total}$. A graphical display of Pearson correlation indices for each variable pair is shown in Supplementary Figure S3. This indicates that $^2\varepsilon_{total}$ is strongly correlated with the relative abundance anteiso-C17:0 fatty acid, and negatively correlated with C16 and C16:1 fatty acid. However, the relative abundance of each of these fatty acids was strongly correlated (negatively, for anteiso-C17:0 fatty acid) with average growth rate (μ). Growth rate emerged as a strong correlate of $^2\varepsilon_{total}$ (**Figure 6**).

DISCUSSION

Hydrogen Isotopes and Intracellular Electron Flow

The aim of this study is to improve our understanding of the influence of intracellular mechanisms that contribute to the $^2H/^1H$ ratios in lipids. Zhang et al. (2009) suggested that mechanisms related to the purine dinucleotide coenzymes NAD(P)H are central to determining δ^2H_{lipid}. In particular, that work suggested that H-isotopic fractionation by transhydrogenase was one potential mechanism for changing the H-isotopic composition of the transferable hydride on NAD(P)H. This is mainly due to the observations that NADPH directly provides up to 50% of lipid hydrogen (Saito et al., 1980; Robins et al., 2003; Schmidt et al., 2003), and predictions that δ^2H_{NADPH} and abundance may vary with growth condition.

Desulfovibrio can generate NADPH via a number of mechanisms. Gram-negative bacteria synthesize $NADP^+$ from NAD^+ by ATP-requiring NAD-kinase, but cannot convert NADH to NADPH via this mechanism (Kawai and Murata, 2008). A number of metabolic reactions reduce $NADP^+$ to generate NADPH. Major intracellular mechanisms of this reduction reaction include a number of hydrogenase/dehydrogenase enzymes within the tricarboxylic acid cycle, the oxidative pentose phosphate pathway, and mixed acid fermentation pathways (Supplementary Table S2). The relative importance of each of these mechanisms varies by substrate, and potential differences in the δ^2H_{NADPH} produced by these different mechanisms has been invoked as a reason for differences in δ^2H_{lipid} (Zhang et al., 2009). Transhydrogenases are another mechanism for NADPH production, catalyzing the transfer of a hydride (H^-) from NADPH to NAD^+, or NADH to $NADP^+$. In addition to the Nfn family of transhydrogenase found in aerobes (Wang et al., 2010), two other families of transhydrogenases are common in

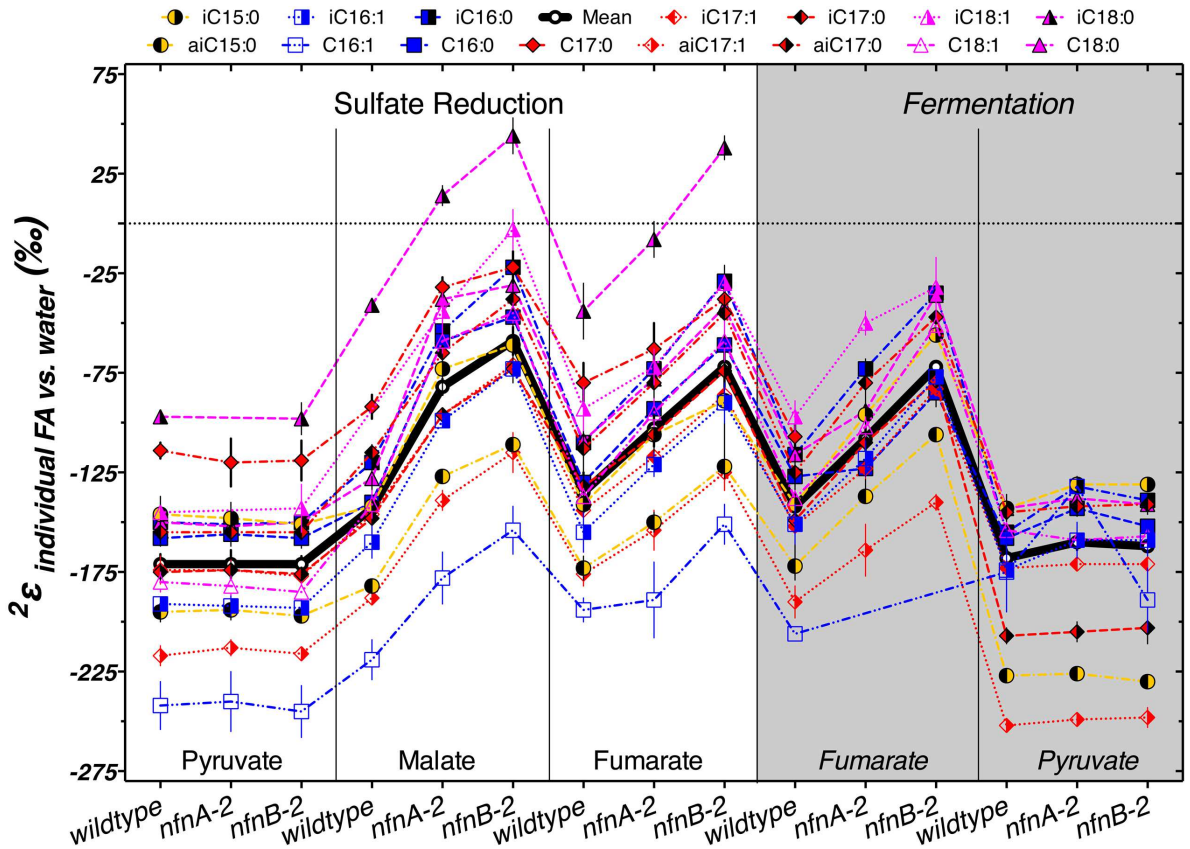

FIGURE 5 | The symbols show the hydrogen isotope fractionation for individual fatty acids, relative to the medium water. The thick horizontal black line represents the mass-weighted fractionation ($^2\varepsilon_{total}$). Each symbol represents the mean of biological replicates ($N = 2$, and technical replication $n_{average} = 3$, range 1–6), with SEM.

aerobes: the proton-translocating transhydrogenase PntAB, and the energy-independent transhydrogenase UdhA (Sauer et al., 2004). These two enzymes have been discussed as a potential mechanism of influencing lipid δ^2H (Zhang et al., 2009; Dawson et al., 2015; Osburn et al., in review). Major mechanisms of NADPH production are summarized by Spaans et al. (2015), and those mechanisms relevant to *D. alaskensis* G20 are summarized in Supplementary Table S2.

Previous work on hydrogen isotope fractionation in sulfate reducing bacteria (SRB) includes studies of pure cultures of *Desulfobacterium autotrophicum* (Campbell et al., 2009; Osburn et al., in review), *Desulfobacter hydrogenophilus* and *D. alaskensis* G20 (Osburn et al., in review) and of *Desulfococcus multivorans* in pure culture and in co-culture with a methanogen (Dawson et al., 2015). Results contrast with those obtained from aerobes, in which growth on different carbon sources results in a large range of $^2\varepsilon_{total}$ (Zhang et al., 2009). *D. Autotrophicum* shows a smaller range in $^2\varepsilon_{total}$ (~45‰) during heterotrophic growth on acetate, succinate, pyruvate, glucose, or formate, or autotrophic growth on H_2/CO_2, yet there are large differences in the $^2\varepsilon_{lipid}$ of individual fatty acids (differences of >100‰) *D. autotrophicum* (Campbell et al., 2009; Osburn et al., in review). *D. hydrogenophilus* and *D. multivorans* grown in pure cultures generate an ~80‰ range in $^2\varepsilon_{total}$ during heterotrophic growth; though when *D. multivorans* was growing in co-culture with the methanogen *Methanosarcina acetivorans* it produced a more muted range in $^2\varepsilon_{total}$ of ~36‰ (Dawson et al., 2015; Osburn et al., in review).

In SRB, transhydrogenase NfnAB plays an important role in energy metabolism (Pereira et al., 2011; Price et al., 2014). If the magnitude of hydrogen isotope fractionation imparted by this transhydrogenase is large, similar to other transhydrogenases, then the activity of this enzyme may play a large role in setting δ^2H_{lipid}. This role may extend to the observed variations in δ^2H_{lipid} as a function of substrate. In this model, NAD(P)H is produced or consumed by a variety of metabolic reactions in the cell (Supplementary Table S2), but cycling of NAD(P)H through NfnAB could play a dominant role in determining the δ^2H of NAD(P)H. The δ^2H_{lipid} might be closely coupled to the size of the pools of oxidized and reduced purine dinucleotide coenzymes, rather than simply a function of changes in NAD(P)H δ^2H. That is, observations of less depleted $^2\varepsilon_{lipid-water}$ may be due to an intracellular isotope distillation effect, where NADPH-hydrogen is more quantitatively transferred to lipids, muting the apparent fractionation. Alternatively, enzymes such as enoyl-ACP (acyl carrier protein) reductase, which are responsible for hydride

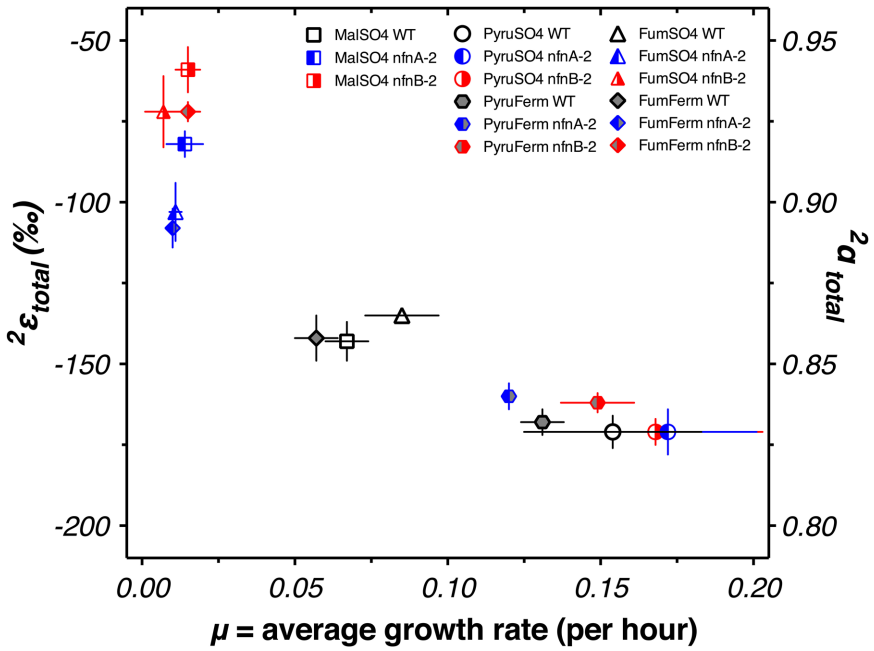

FIGURE 6 | Average weighted growth rate (μ) versus the $^2\varepsilon_{total}$ for all experiments.

transfer during fatty acid biosynthesis may be capable of utilizing either NADH and NADPH (Bergler et al., 1996), and the preferred substrate may change depending on their relative pool size. The perturbation of NfnAB in mutant strains would be expected to affect the relative sizes of these pools, and could help explain the observed patterns in lipids.

If NfnAB is important in determining δ^2H_{lipid} in SRB, it could also be significant in other anaerobes as well. NfnAB genes are widely distributed in anaerobes, particularly in Deltaproteobacteria, Thermotogae, Clostridia, and methanogenic archaea (Buckel and Thauer, 2013), and thus far ubiquitous in sulfate-reducing bacteria (this study, Pereira et al., 2011). **Figure 7** shows the relationship of NfnAB sequences from a range of anaerobes. Interestingly, all the SRB measured for lipid/water H-isotope fractionation to-date (Sessions et al., 1999; Campbell et al., 2009; Dawson et al., 2015; Osburn et al., in review) contain some form of the NfnAB. While *nfnAB* sequences tend to cluster phylogenetically, the gene tree shown in **Figure 7** identifies potential lateral gene transfer events among the SRB. The NfnAB genes from *Desulfobulbus propionicus* and *Syntrophobacter fumaroxidans* are more similar to those of the methanogenic archaea rather than the other SRB in the Deltaproteobacteria (including *D. alaskensis* G20), which cluster together. Similar to *D. alaskensis* G20, *D. propionicus* and *S. fumaroxidans* are SRB that are capable of fermentative growth on compounds such pyruvate (both) and fumarate (*S. fumaroxidans*).

In *D. alaskensis* G20, the catalytic role of the NfnAB transhydrogenase shows a relationship to the δ^2H_{lipid} patterns. During growth on pyruvate/sulfate, electrons are predicted to flow from pyruvate to ferredoxin, then from ferredoxin through NfnAB to produce reduced NADPH (Price et al., 2014). That study pointed out that the reaction of transhydrogenase is probably required to produce sufficient NADPH for biosynthesis, even though the experiments were done in the presence of yeast extract, which minimized the importance of this reaction. In contrast, our isotopic experiments used a defined medium lacking yeast extract, so the importance of the transhydrogenase reaction would be even greater. For both the wild type and mutant, growth on pyruvate/sulfate produced lipids that uniformly had the most negative $^2\varepsilon_{total}$ across all our experiments. This experiment showed no phenotype for the *nfn* mutants, either in isotopic composition or in growth rate.

Sulfate reduction using malate likely employs NfnAB-2 to produce NADPH by oxidizing NADH and reduced ferredoxin (Price et al., 2014). Fumarate respiration operates in a manner similar to malate. These two substrates can be interconverted by fumarase (Price et al., 2014), so this similarity is likely to be related to similar growth and electron flow. Growth on each of these substrates produces similar patterns in hydrogen isotope fractionation. In each case, the wild type strain produces lipids with $^2\varepsilon_{total}$ near −140‰, which is not as depleted in deuterium as lipids produced during growth on pyruvate. In contrast to growth on pyruvate, the mutant strains produce substantially less depleted lipids, resulting in a lesser degree of fractionation ($^2\varepsilon_{total}$) than the wild type. One explanation for this difference is that the mutation of one paralog of NfnAB in this strain changed the ratio of reduced to oxidized dinucleotides in the cell, with a higher ratio of NADPH to $NADP^+$ and a lower ratio of NADH to NAD^+. A second possibility is that the change in $^2\varepsilon_{total}$ is a consequence of the growth defect of the mutant strains.

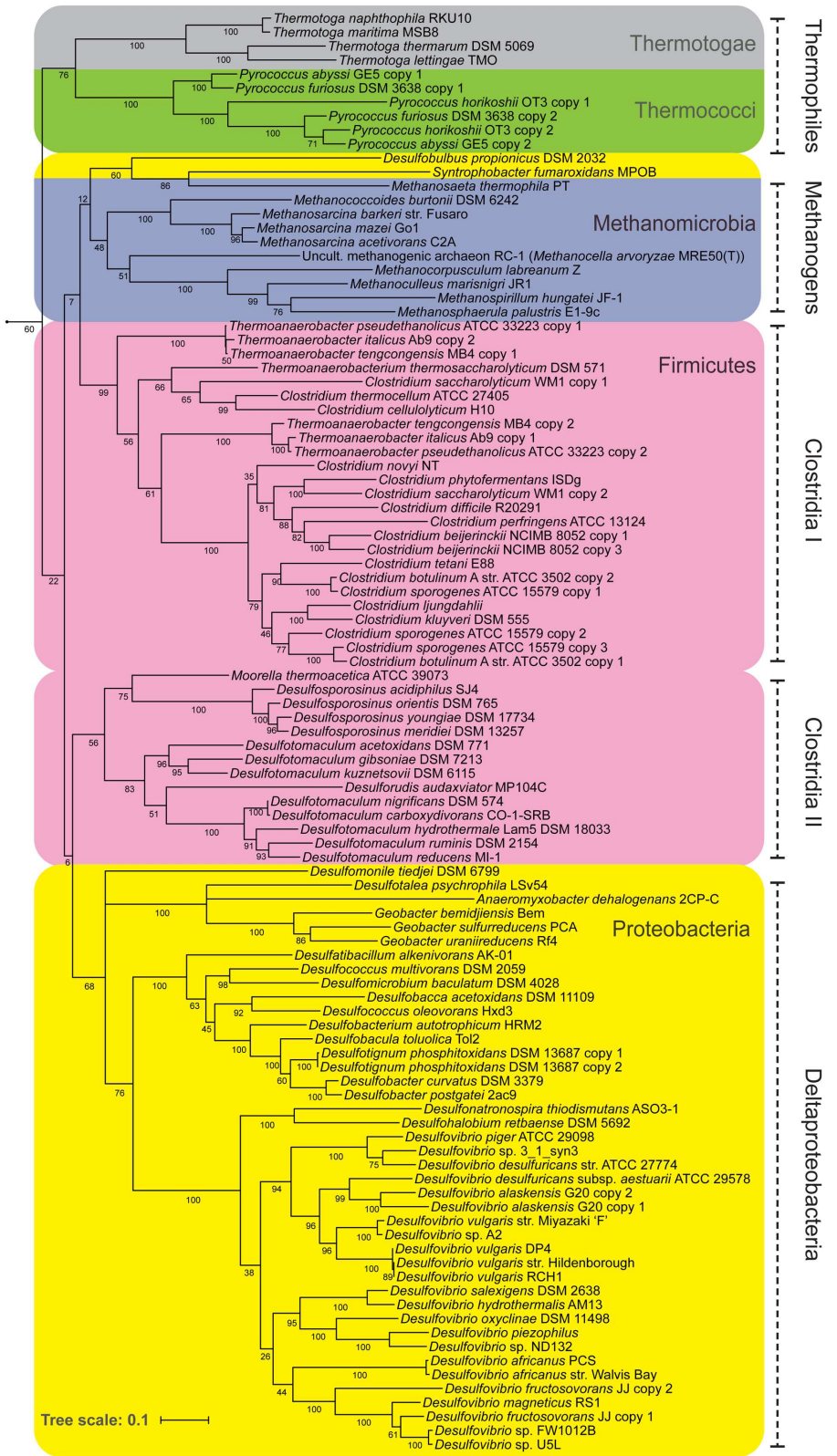

FIGURE 7 | A maximum likelihood phylogenetic tree of NfnAB using amino acid sequences taken from the sequenced genomes of known anaerobes. Each branch is colored by Phylum. Bootstrap values (out of 100) are shown at each branch point.

Previous work has investigated the relationship of growth rate to $^{2}\varepsilon_{total}$. Zhang et al. (2009) did not observe a systematic relationship in the aerobic organisms that they studied. However, a negative relationship was observed between growth rate and the water–alkenone hydrogen isotope fractionation in the coccolithophores *Emiliania huxleyi* and *Gephyrocapsa oceanica* (Schouten et al., 2006; Sachs and Kawka, 2015). This observation is similar to that reported here, although the slope is steeper for *D. alaskensis* G20. Microbial lipids were recently reported to change their $\delta^{2}H_{lipid}$ with growth phase (Heinzelmann et al., 2015), although this effect was relatively minor. Algal lipids have been reported to modulate $\delta^{2}H_{lipid}$ as a function of physiological state (Estep and Hoering, 1980; Romero-Viana et al., 2013). Each of these relationships could be conceivably related to changes in the turnover rate or ratios of intracellular metabolites, but specific metabolomics data elucidating these relationships has yet to be produced.

Fermentation of pyruvate by *D. alaskensis* G20 likely involves the reduction of pyruvate with NADH by malic enzyme (ME; Dde_1253) to malate (Meyer et al., 2014), which is then dehydrated by fumarase to fumarate, and then reduced to succinate (see Price et al., 2014). The oxidative branch of this fermentation involves the transformation of pyruvate to acetate, which reduces ferredoxin. Reduced ferredoxin is recycled via flavin-based electron bifurcation, catalyzed by Hdr-Flox-1 (Meyer et al., 2014), but may also interact with NfnAB in the same way as during pyruvate respiration, in an electron confurcation reaction involving NADH, producing NADPH. Wild type *D. alaskensis* G20 grown by pyruvate fermentation produced lipids that showed $^{2}\varepsilon_{total}$ comparable to that produced during pyruvate respiration. However, the *nfnAB-2* mutants grown by pyruvate fermentation generated an $^{2}\varepsilon_{total}$ slightly more enriched than the wild type (**Figure 4**, mutants: −160‰ and −162‰, relative to wild type: −168‰). If the *nfnAB-2* mutation inhibited NADPH formation, this pattern is opposite of that seen in other experiments, as it results in less fractionation (less negative $^{2}\varepsilon_{total}$) at a lower predicted NADPH/NADP ratio. Nonetheless, the shift is minimal (<10‰) and the important reactions in ferredoxin recycling may be complicating this interpretation. Unlike the result in Meyer et al. (2014), *nfnAB-2* mutants in our experiments did not show a growth defect on pyruvate fermentation. This may in part be related to partial pressures of H_2 produced by growing strains (not monitored herein). Alternatively, this may be due to the presence of the second transhydrogenase in G20, *nfnAB-1*, as highlighted above with respect to the pyruvate/sulfate experiments.

Fumarate fermentation in SRB is not well studied, but it is likely a complex metabolism. Wild type *D. alaskensis* G20 has nearly identical growth rates during fumarate fermentation and respiration. The *nfn* mutants grow more slowly than the wild type, but show little difference between fumarate fermentation and respiration. Respiration and fermentation of fumarate, along with respiration of malate, show nearly identical patterns in growth rate and in $^{2}\varepsilon_{total}$ for each of our three strains (**Figure 4**). This suggests an underlying mechanism uniting these growth conditions.

Fatty acid profiles across the three strains and five conditions show some correlations with the total isotopic fractionation (Supplementary Figure S3). The fractional abundance of branched chain lipids, particularly anteiso-C17:0, is positively correlated with the fractionation and negatively correlated with growth rate. We can reason two ways in which changing $\delta^{2}H$ values of fatty acids may result in a less negative $^{2}\varepsilon_{total}$ (Supplementary Figure S2). The isotopic ordering of lipids may be altered, resulting in a net change in $^{2}\varepsilon_{total}$; alternatively, there could be a consistent shift in the $^{2}\varepsilon_{lipid}$ of most or all lipids. Data shown in **Figures 3** and **5** rule out the first option, and show that almost all individual $^{2}\varepsilon_{lipid}$ change in concert between conditions. This suggests that the driving mechanism for changes in $^{2}\varepsilon_{total}$ relates to processes relevant to all lipids. The processes related to the production and consumption of NADPH are consistent with this role.

Integrating data from all five experimental conditions and three strains suggests a relationship between growth rate and $^{2}\varepsilon_{total}$ (**Figure 6**). We do not yet have a theoretical prediction for the nature of this relationship, but the relationship is consistent with a linear, exponential decay, or hyperbolic relationship between growth rate and isotope fractionation. This pattern is similar, although opposite in sign, to that seen in sulfur isotope fractionation imposed by SRB during dissimilatory sulfate reduction (Kaplan and Rittenberg, 1964; Chambers et al., 1975; Sim et al., 2011, 2013; Leavitt et al., 2013). Models aimed at addressing the growth rate—fractionation relationship in sulfur isotopes have focused on ratios of intracellular metabolites and redox state (Wing and Halevy, 2014; Bradley et al., 2016). Similar controls could be at work in controlling hydrogen isotope fractionation: ratios of $NAD(P)H/NAD(P)^{+}$ and intracellular redox state are related and the partitioning of hydrogen between these pools could exert a direct effect on $\delta^{2}H_{lipid}$. However, we cannot rule out the possibility that the correlation with growth rate is fortuitous, and correlations between $\delta^{2}H_{lipid}$ and growth rate have not been observed in other studies (Zhang et al., 2009; Dawson et al., 2015). Ongoing work is aimed at testing this hypothesis, through growth of SRB in chemostats. If this hypothesis holds, then $^{2}\varepsilon_{total}$ and $\delta^{2}H_{lipid}$ of sulfate reducers may be able to provide a critical constraint on the interpretation of sulfur isotope patterns in natural systems, such as marine sediments and anoxic water columns.

Transhydrogenases related to *nfnAB* are widely distributed in anaerobes (**Figure 7**), and reactions catalyzed by this class of transhydrogenase may influence sedimentary lipid H-isotopic distributions in a wide range of natural settings. The metabolic role of NfnAB has been investigated in other anaerobes, notably thermophilic Clostridia (Lo et al., 2015), and similar studies of hydrogen isotope fractionation using these strains may indicate whether the patterns uncovered here in sulfate reducers are more generally applicable throughout obligate anaerobes, and the microbial domains of life in general.

The biggest differences in $\delta^{2}H$ that we observe in these experiments are not between growth on various substrates or

between wild type and mutant, but among individual fatty acids grown in a single culture. Understanding the biosynthetic mechanisms that are driving these differences will be key to the interpretations of the isotopic compositions of sedimentary fatty acids. The isotopic ordering is consistent, and differences in $^2\varepsilon_{total}$ are not driven by changing abundances of lipids with extreme δ^2H_{lipid}, but by systematic changes across all lipids (**Figure 5**; Supplementary Figure S2).

The enrichment in δ^2H_{lipid} of saturated fatty acids relative to their unsaturated homologs may be tied to biosynthesis. During fatty acid elongation, double bonds are introduced during each successive two-carbon addition. These *trans* double bonds are reduced by enoyl-ACP reductase, FabI (Kass and Bloch, 1967). A *trans* to *cis* configurational change can be introduced to the 10-carbon intermediate, preventing the function of FabI and conserving the double bond during further chain elongation. Fatty acids that have undergone this conversion are depleted in δ^2H_{lipid}, suggesting that the hydrogen transferred by FabI during fatty acid elongation is enriched in δ^2H relative to average δ^2H_{lipid}. However, we cannot rule out the possibility that saturated and unsaturated fatty acids were produced at different times in the growth of our cultures and that the isotopic differences may reflect a different process than that articulated here. Enrichment of saturated fatty acids relative to their unsaturated homologs has been previously observed in marine macroalgae (Chikaraishi et al., 2004). That observation was attributed to a hydrogen isotope fractionation imposed during desaturation of fatty acids, leaving residual saturated fatty acids enriched in deuterium. This mechanism is plausible in eukaryotes, where fatty acid desaturation is accomplished by an oxygen-dependent desaturase that operates on a fully elongated saturated fatty acid (Harwood and Guschina, 2009). However, this mechanism cannot explain similar patterns in bacteria.

Another observation necessitating explanation is the depletion in δ^2H_{lipid} of anteiso-branched fatty acids relative to the straight chain fatty acids (Supplementary Figure S2). Biosynthesis offers a potential explanation here as well. Straight-chain fatty acids are extended two carbons at a time by successive transfers of acetyl units (transferred as malonyl-ACP with the loss of CO_2 during each transfer). The primer for this chain extension is acetyl-CoA in the case of straight chain fatty acids, but differs for iso- and anteiso-branched fatty acids (Kaneda, 1991). Even-numbered iso-branched fatty acids use isobutyryl-CoA (derived from valine) as a primer, while odd-numbered iso-branched fatty acids use isovaleryl-CoA (derived from leucine). Odd-numbered anteiso-branched fatty acids use 2-methylbutyryl-CoA (derived from isoleucine) as a primer (Kaneda, 1991). One possible explanation for a δ^2H-depletion in anteiso-branched fatty acids is a depletion in the δ^2H content of isoleucine. Isoleucine contributes nine hydrogen atoms to anteiso-branched fatty acids, roughly 25% of all non-exchangeable hydrogen in anteiso-C15 or -C17 fatty acids. A deuterium depletion in isoleucine might explain the observed patterns. Mass balance calculations suggest that for this to be the case isoleucine would need to be depleted relative to water by −120‰ to −300‰ among the various experiments. Depletions as large as 300‰ would be exceptionally large, and might be cause to invoke a different mechanism to explain the patterns seen here. Nonetheless, the prediction of deuterium-depleted isoleucine could be tested by compound-specific analysis of amino acid δ^2H. This has been only recently been developed as an analytical technique, but initial results suggest large differences in the δ^2H content of various amino acids (Fogel et al., 2015). Such an approach could prove powerful in understanding the diversity of δ^2H_{lipid} values produced by individual organisms.

CONCLUSION

The magnitude of hydrogen isotope fractionation in *D. alaskensis* G20 is influenced by the growth substrate, with growth on pyruvate exhibiting a different isotopic phenotype than growth on other substrates. Large differences are observed in the δ^2H_{lipid} among individual lipids under all conditions. These differences may relate to biosynthesis, but are not fully accounted for. Wild type and *nfnAB-2* mutants show large differences in $^2\varepsilon_{total}$ under conditions in which NfnAB-2 is predicted to play a significant role in energy conservation. This phenotype was observed across the entirety of the *D. alaskensis* G20 fatty acid profile. While $^2\varepsilon_{total}$ correlates with modest changes in the fatty acids produced, it cannot be accounted for by changes in the abundance of individual lipids. These changes in apparent fractionation indicate a role for NfnAB-2 in determining both growth rate and δ^2H_{lipid} for *D. alaskensis* G20, particularly when grown on malate or fumarate. NfnAB is widely distributed in anaerobes, and may play a role in determining δ^2H_{lipid} in other organisms. Future work will aim to isolate these variables and further strengthen our understanding of the roles of growth and metabolic rate, substrate-induced differences in energy conservation pathways, and expression of transhydrogenase as key factors in determining the hydrogen isotope ratios of lipids.

AUTHOR CONTRIBUTIONS

WL and AB designed the project. WL performed the growth experiments, with guidance from AB. WL and MS performed sample analysis. Data analysis was performed by WL and AB with input from MS. TF designed and conducted all phylogenetic analyses. WL and AB wrote the manuscript with input from TF and expert editorial input from MS.

FUNDING

This work was funded by NASA Exobiology grant 13-EXO13-0082 (AB, WL). WL acknowledges Washington University for the Steve Fossett Postdoctoral Fellowship. TF acknowledges support from the Subsurface Science Scientific Focus Area at Argonne National Laboratory supported by the Subsurface Biogeochemical Research Program, U.S. Department of Energy (DOE) Office of Science, Office of Biological and Environmental Research, under DOE contract DE-AC02-06CH11357.

ACKNOWLEDGMENTS

We thank Dr. A. Deutschbauer and Dr. J. Ray (Lawrence Berkeley National Laboratory) for providing *D. alaskensis* G20 mutant and wild type strains, Dr. M. Osburn (Northwestern University) for water H isotope measurements and discussions of our data, and Dr. M. Lefticariu (Southern Illinois University, Carbondale) for external verification of lab H isotope standards. We also thank undergraduate researchers C. Wallace and L. Johnson (Washington University in St. Louis) for laboratory assistance.

SUPPLEMENTARY MATERIAL

The Supplementary Material for this article can be found online at: http://journal.frontiersin.org/article/10.3389/fmicb.2016.00918, and at http://dx.doi.org/10.6084/m9.figshare.2132731.

REFERENCES

Bergler, H., Fuchsbichler, S., Högenauer, G., and Turnowsky, F. (1996). The enoyl-[acyl-carrier-protein] reductase (FabI) of *Escherichia coli*, which catalyzes a key regulatory step in fatty acid biosynthesis, accepts NADH and NADPH as cofactors and is inhibited by palmitoyl-CoA. *Eur. J. Biochem.* 242, 689–694. doi: 10.1111/j.1432-1033.1996.0689r.x

Bizouarn, T., Grimley, R. L., Cotton, N. P. J., Stilwell, S. N., Hutton, M., and Jackson, J. B. (1995). The involvement of NADP(H) binding and release in energy transduction by proton-translocating nicotinamide nucleotide transhydrogenase from *Escherichia coli*. *Biochim. Biophys. Acta Bioenerg.* 1229, 49–58. doi: 10.1016/0005-2728(94)00186-9

Bradley, A. S., Leavitt, W. D., Schmidt, M., Knoll, A. H., Girguis, P. R., and Johnston, D. T. (2016). Patterns of sulfur isotope fractionation during microbial sulfate reduction. *Geobiology* 14, 91–101. doi: 10.1111/gbi.12149

Buckel, W., and Thauer, R. K. (2013). Energy conservation via electron bifurcating ferredoxin reduction and proton/Na+ translocating ferredoxin oxidation. *Biochim. Biophys. Acta Bioenerg.* 1827, 94–113. doi: 10.1016/j.bbabio.2012.07.002

Campbell, B. J., Li, C., Sessions, A. L., and Valentine, D. L. (2009). Hydrogen isotopic fractionation in lipid biosynthesis by H2-consuming *Desulfobacterium autotrophicum*. *Geochim. Cosmochim. Acta* 73, 2744–2757. doi: 10.1016/j.gca.2009.02.034

Chambers, L. A., Trudinger, P. A., Smith, J. W., and Burns, M. S. (1975). Fractionation of sulfur isotopes by continuous cultures of *Desulfovibrio desulfuricans*. *Can. J. Microbiol.* 21, 1602–1607. doi: 10.1139/m75-234

Chikaraishi, Y., Naraoka, H., and Poulson, S. R. (2004). Hydrogen and carbon isotopic fractionations of lipid biosynthesis among terrestrial (C3, C4 and CAM) and aquatic plants. *Phytochemistry* 65, 1369–1381. doi: 10.1016/j.phytochem.2004.03.036

Coplen, T. B., Böhlke, J. K., De Biévre, P., Ding, T., Holden, N. E., Hopple, J. A., et al. (2002). Isotope-abundance variations of selected elements (IUPAC Technical Report). *Pure Appl. Chem.* 74, 1987–2017. doi: 10.1351/pac200274101987

Dawson, K. S., Osburn, M. R., Sessions, A. L., and Orphan, V. J. (2015). Metabolic associations with archaea drive shifts in hydrogen isotope fractionation in sulfate-reducing bacterial lipids in cocultures and methane seeps. *Geobiology* 13, 462–477. doi: 10.1111/gbi.12140

Dickschat, J. S., Bruns, H., and Riclea, R. (2011). Novel fatty acid methyl esters from the actinomycete *Micromonospora aurantiaca*. *Beilstein J. Org. Chem.* 7, 1697–1712. doi: 10.3762/bjoc.7.200

Edgar, R. C. (2004). MUSCLE: multiple sequence alignment with high accuracy and high throughput. *Nucleic Acids Res.* 32, 1792–1797. doi: 10.1093/nar/gkh340

Estep, M. F., and Hoering, T. C. (1980). Biogeochemistry of the stable hydrogen isotopes. *Geochim. Cosmochim. Acta* 44, 1197–1206. doi: 10.1016/0016-7037(80)90073-3

Fogel, M. L., Newsome, S. D., Griffin, P., Bradley, C. J., and Graves, G. R. (2015). "Hydrogen isotopes in amino acids: more than just precipitation tracers," in *Proceedings of the 27th International Meeting on Organic Geochemistry*, Prague, 60.

Harwood, J. L., and Guschina, I. A. (2009). The versatility of algae and their lipid metabolism. *Biochimie* 91, 679–684. doi: 10.1016/j.biochi.2008.11.004

Hayes, J. M. (2001). "Fractionation of the isotopes of carbon and hydrogen in biosynthetic processes," in *Stable Isotope Geochemistry, Reviews in Mineralogy and Geochemistry* Vol. 43, eds J. W. Valley and D. R. Cole (Washington, DC: Mineralogical Society of America), 225–278.

Heinzelmann, S. M., Villanueva, L., Sinke-Schoen, D., Sinninghe Damsté, J. S., Schouten, S., and van der Meer, M. T. J. (2015). Impact of metabolism and growth phase on the hydrogen isotopic composition of microbial fatty acids. *Front. Microbiol.* 6:408. doi: 10.3389/fmicb.2015.00408

Jackson, J. B. (2003). Proton translocation by transhydrogenase. *FEBS Lett.* 545, 18–24. doi: 10.1016/S0014-5793(03)00388-0

Jackson, J. B., Peake, S. J., and White, S. A. (1999). Structure and mechanism of proton-translocating transhydrogenase. *FEBS Lett.* 464, 1–8. doi: 10.1016/S0014-5793(99)01644-0

Kaneda, T. (1991). Iso- and Anteiso-Fatty acids in bacteria: biosynthesis, function, and taxonomic significance. *Microbiol. Rev.* 55, 288–302.

Kaplan, I. R., and Rittenberg, S. C. (1964). Microbiological fractionation of sulphur isotopes. *J. Gen. Microbiol.* 34, 195–212. doi: 10.1099/00221287-34-2-195

Kass, L. R., and Bloch, K. (1967). On the enzymatic synthesis of unsaturated fatty acids in *Escherichia coli*. *Proc. Natl. Acad. Sci. U.S.A.* 58, 1168–1173. doi: 10.1073/pnas.58.3.1168

Kawai, S., and Murata, K. (2008). Structure and function of NAD kinase and NADP phosphatase: key enzymes that regulate the intracellular balance of NAD(H) and NADP(H). *Biosci. Biotechnol. Biochem.* 72, 919–930. doi: 10.1271/bbb.70738

Kuehl, J. V., Price, M. N., Ray, J., Wetmore, K. M., Esquivel, Z., and Kazakov, A. E. (2014). Functional genomics with a comprehensive library of transposon mutants for the sulfate-reducing bacterium *Desulfovibrio alaskensis* G20. *MBio* 5:e1041-14. doi: 10.1128/mBio.01041-14 e1041-14

Larsson, A. (2014). AliView: a fast and lightweight alignment viewer and editor for large datasets. *Bioinformatics* 30, 3276–3278. doi: 10.1093/bioinformatics/btu531

Leavitt, W. D., Halevy, I., Bradley, A. S., and Johnston, D. T. (2013). Influence of sulfate reduction rates on the Phanerozoic sulfur isotope record. *Proc. Natl. Acad. Sci. U.S.A.* 110, 11244–11249. doi: 10.1073/pnas.1218874110

Letunic, I., and Bork, P. (2011). Interactive tree of life v2: online annotation and display of phylogenetic trees made easy. *Nucleic Acids Res.* 39, 475–478. doi: 10.1093/nar/gkr201

Lo, J., Zheng, T., Olson, D. G., Ruppertsberger, N., Tripathi, S. A., Guss, A. M., et al. (2015). Deletion of nfnAB in *Thermoanaerobacterium saccharolyticum* and its effect on metabolism. *J. Bacteriol.* 197, 3367. doi: 10.1128/JB.00347-15

Markowitz, V. M., Chen, I. M. A., Palaniappan, K., Chu, K., Szeto, E., Grechkin, Y., et al. (2012). IMG: the integrated microbial genomes database and comparative analysis system. *Nucleic Acids Res.* 40, 115–122. doi: 10.1093/nar/gkr1044

Marti-Renom, M. A., Stuart, A. C., Fiser, A., Sánchez, R., Melo, F., and Sali, A. (2000). Comparative protein structure modeling of genes and genomes. *Annu. Rev. Biophys. Biomol. Struct.* 29, 291–325. doi: 10.1146/annurev.biophys.29.1.291

Meyer, B., Kuehl, J. V., Price, M. N., Ray, J., Deutschbauer, A. M., Arkin, A. P., et al. (2014). The energy-conserving electron transfer system used by *Desulfovibrio alaskensis* strain G20 during pyruvate fermentation involves reduction of endogenously formed fumarate and cytoplasmic and membrane-bound complexes, Hdr-Flox and Rnf. *Environ. Microbiol.* 16, 3463–3486. doi: 10.1111/1462-2920.12405

Nichols, P. D., Guckert, J. B., and White, D. C. (1986). Determination of monosaturated fatty acid double-bond position and geometry for microbial monocultures and complex consortia by capillary GC-MS of their dimethyl

disulphide adducts. *J. Microbiol. Methods* 5, 49–55. doi: 10.1016/0167-7012(86)90023-0

Overbeek, R., Olson, R., Pusch, G. D., Olsen, G. J., Davis, J. J., Disz, T., et al. (2014). The SEED and the rapid annotation of microbial genomes using subsystems technology (RAST). *Nucleic Acids Res.* 42, 1–9. doi: 10.1093/nar/gkt1226

Pearson, A. (2014). "Lipidomics for Geochemistry," in *Treatise on Geochemistry: 2nd Edn*, eds H. D. Holland and K. K. Turekian (Oxford: Elsevier), 291–336.

Pereira, I. A. C., Ramos, A. R., Grein, F., Marques, M. C., da Silva, S. M., and Venceslau, S. S. (2011). A comparative genomic analysis of energy metabolism in sulfate reducing bacteria and archaea. *Front. Microbiol.* 2:69. doi: 10.3389/fmicb.2011.00069

Polissar, P. J., and D'Andrea, W. J. (2014). Uncertainty in paleohydrologic reconstructions from molecular δD values. *Geochim. Cosmochim. Acta* 129, 146–156. doi: 10.1016/j.gca.2013.12.021

Price, M. N., Ray, J., Wetmore, K. M., Kuehl, J. V., Bauer, S., and Deutschbauer, A. M. (2014). The genetic basis of energy conservation in the sulfate-reducing bacterium *Desulfovibrio alaskensis* G20. *Front. Microbiol.* 5:577. doi: 10.3389/fmicb.2014.00577

Qi, H., and Coplen, T. B. (2011). Investigation of preparation techniques for δ2H analysis of keratin materials and a proposed analytical protocol. *Rapid Commun. Mass Spectrom.* 25, 2209–2222.

Rabus, R., Hansen, T. A., and Widdel, F. (2006). "Dissimilatory sulfate- and sulfur-reducing prokaryotes," in *The Prokaryotes*, eds M. Dworkin, S. Falkow, E. Rosenberg, K.-H. Schleifer, and E. Stackebrandt (New York, NY: Springer), 659–768.

Rabus, R., Venceslau, S. S., Wöhlbrand, L., Voordouw, G., Wall, J. D., and Pereira, I. A. C. (2015). A post-genomic view of the ecophysiology, catabolism and biotechnological relevance of sulphate-reducing prokaryotes. *Adv. Microb. Physiol.* 66, 55–321.

R Core Team (2015). *R: A Language and Environment for Statistical Computing*. Vienna: R Foundation for Statistical Computing.

Robins, R. J., Billault, I., Duan, J. R., Guiet, S., Pionnier, S., and Zhang, B. L. (2003). Measurement of 2H distribution in natural products by quantitative 2H NMR: an approach to understanding metabolism and enzyme mechanism? *Phytochem. Rev.* 2, 87–102. doi: 10.1023/B:PHYT.0000004301.52646.a8

Rodriguez-Ruiz, J., Belarbi, E., Sanchez, L. G., and Diego, L. (1998). Rapid simultaneous lipid extraction and transesterification for fatty acid analyses. *Biotechnol. Tech.* 12, 689–691.

Romero-Viana, L., Kienel, U., Wilkes, H., and Sachse, D. (2013). Growth-dependent hydrogen isotopic fractionation of algal lipid biomarkers in hypersaline Isabel Lake (Mexico). *Geochim. Cosmochim. Acta* 106, 490–500. doi: 10.1016/j.gca.2012.12.017

Rost, B. (1999). Twilight zone of protein sequence alignments. *Protein Eng.* 12, 85–94. doi: 10.1093/protein/12.2.85

Sachs, J. P., and Kawka, O. E. (2015). The influence of growth rate on $^{2}H/^{1}H$ fractionation in continuous cultures of the coccolithophorid *Emiliania huxleyi* and the diatom *Thalassiosira pseudonana*. *PLoS ONE* 10:e0141643. doi: 10.1371/journal.pone.0141643

Saito, K., Kawaguchi, A., Okuda, S., Seyama, Y., and Yamakawa, T. (1980). Incorporation of hydrogen atoms from deuterated water and stereospecifically deuterium-labeled nicotinamide nucleotides into fatty acids with the *Escherichia coli* fatty acid synthetase system. *Biochim. Biophys. Acta* 618, 202–213. doi: 10.1016/0005-2760(80)90026-0

Sauer, P. E., Eglinton, T. I., Hayes, J. M., Schimmelmann, A., and Sessions, A. L. (2001). Compound-specific D/H ratios of lipid biomarkers from sediments as a proxy for environmental and climatic conditions. *Geochim. Cosmochim. Acta* 65, 213–222. doi: 10.1016/S0016-7037(00)00520-2

Sauer, U., Canonaco, F., Heri, S., Perrenoud, A., and Fischer, E. (2004). The soluble and membrane-bound transhydrogenases UdhA and PntAB have divergent functions in NADPH metabolism of *Escherichia coli*. *J. Biol. Chem.* 279, 6613–6619. doi: 10.1074/jbc.M311657200

Schmidt, H.-L., Werner, R. A., and Eisenreich, W. (2003). Systematics of 2H patterns in natural compounds and its importance for the elucidation of biosynthetic pathways. *Phytochem. Rev.* 2, 61–85. doi: 10.1023/B:PHYT.0000004185.92648.ae

Schouten, S., Ossebaar, J., Schreiber, K., Kienhuis, M. V. M., Langer, G., Benthien, A., et al. (2006). The effect of temperature, salinity and growth rate on the stable hydrogen isotopic composition of long chain alkenones produced by *Emiliania huxleyi* and *Gephyrocapsa oceanica*. *Biogeosciences* 3, 113–119. doi: 10.5194/bg-3-113-2006

Sessions, A. L., Burgoyne, T. W., Schimmelmann, A., and Hayes, J. M. (1999). Fractionation of hydrogen isotopes in lipid biosynthesis. *Org. Geochem.* 30, 1193–1200. doi: 10.1016/S0146-6380(99)00094-7

Sessions, A. L., and Hayes, J. M. (2005). Calculation of hydrogen isotopic fractionations in biogeochemical systems. *Geochim. Cosmochim. Acta* 69, 593–597. doi: 10.1016/j.gca.2004.08.005

Silvestro, D., and Michalak, I. (2012). RaxmlGUI: a graphical front-end for RAxML. *Org. Divers. Evol.* 12, 335–337. doi: 10.1007/s13127-011-0056-0

Sim, M. S., Bosak, T., and Ono, S. (2011). Large sulfur isotope fractionation does not require disproportionation. *Science* 333, 74–77. doi: 10.1126/science.1205103

Sim, M. S., Wang, D. T., Zane, G. M., Wall, J. D., Bosak, T., and Ono, S. (2013). Fractionation of sulfur isotopes by Desulfovibrio vulgaris mutants lacking hydrogenases or type I tetraheme cytochrome c 3. *Front. Microbiol.* 4:171. doi: 10.3389/fmicb.2013.00171

Smith, B. N., and Epstein, S. (1970). Biogeochemistry of the stable isotopes of hydrogen and carbon in salt marsh biota. *Plant Physiol.* 46, 738–742. doi: 10.1104/pp.46.5.738

Spaans, S. K., Weusthuis, R. A., van der Oost, J., and Kengen, S. W. M. (2015). NADPH-generating systems in bacteria and archaea. *Front. Microbiol.* 6, 1–27

Stamatakis, A. (2006). RAxML-VI-HPC: maximum likelihood-based phylogenetic analyses with thousands of taxa and mixed models. *Bioinformatics* 22, 2688–2690. doi: 10.1093/bioinformatics/btl446

Taylor, J., and Parkes, R. J. (1983). The cellular fatty acids of the sulphate-reducing bacteria, *Desulfobacter* sp., *Desulfobulbus sp*. and *Desulfovibrio desulfuricans*. *J. Gen. Microbiol.* 129, 3303–3309.

Venning, J. D., Bizouarn, T., Cotton, N. P. J., Quirk, P. G., and Jackson, J. B. (1998). Stopped-flow kinetics of hydride transfer between nucleotides by recombinant domains of proton-translocating transhydrogenase. *Eur. J. Biochem.* 257, 202–209. doi: 10.1046/j.1432-1327.1998.2570202.x

Wang, S., Huang, H., Moll, J., Thauer, R. K., Al, W. E. T., and Acteriol, J. B. (2010). NADP+ reduction with reduced ferredoxin and NADP+ reduction with NADH are coupled via an electron-bifurcating enzyme complex in *Clostridium kluyveri*. *J. Bacteriol.* 192, 5115–5123. doi: 10.1128/JB.00612-10

Wing, B. A., and Halevy, I. (2014). Intracellular metabolite levels shape sulfur isotope fractionation during microbial sulfate respiration. *Proc. Natl. Acad. Sci. U.S.A.* 111, 18116–18125. doi: 10.1073/pnas.1407502111

Zhang, X., Gillespie, A. L., and Sessions, A. L. (2009). Large D/H variations in bacterial lipids reflect central metabolic pathways. *Proc. Natl. Acad. Sci. U.S.A.* 106, 12580–12586. doi: 10.1073/pnas.0903030106

Conflict of Interest Statement: The authors declare that the research was conducted in the absence of any commercial or financial relationships that could be construed as a potential conflict of interest.